International Journal of Thermal Sciences 192 (2023) 108428

Contents lists available at ScienceDirect

International Journal of Thermal Sciences

journal homepage: www.elsevier.com/locate/ijts

TiN-based metasurface absorber for efficient solar energy harvesting

Bing Yang [a], Yuan Zou [b], Kun Zhou [c], Haotuo Liu [d], Xiaohu Wu [d,*]

[a] *Centre for Advanced Laser Manufacturing (CALM), School of Mechanical Engineering, Shandong University of Technology, Zibo, 255000, PR China*
[b] *College of Electromechanical Engineering, Qingdao University of Science and Technology, Qingdao, 266061, PR China*
[c] *School of Safety Engineering, China University of Mining and Technology, Xuzhou, 221116, PR China*
[d] *Shandong Institute of Advanced Technology, Jinan, 250100, PR China*

A R T I C L E I N F O

Keywords:
Metasurface absorber
Titanium nitride
Surface plasmon resonance
Fabry-Pérot resonance
Solar energy harvesting

A B S T R A C T

Solar absorber, which is widely used in concentrated solar thermal systems and solar photovoltaics, has attracted great attention in recent years. Concentrated solar irradiation not only saves production costs, but also effectively improves the photothermal conversion efficiency of the system. However, the huge radiative heat flux will cause the system temperature to rise rapidly, which poses significant challenges for designing solar absorbers. Here, a metasurface absorber based on cylinder array structure is proposed for efficient solar energy harvesting, using the high-temperature resistant materials TiN and SiO_2. The total solar absorption of the absorber is up to 0.94 at wavelengths of 300–2500 nm. The high absorption performance of the metasurface absorber can be explained as the coupling effect of surface plasmon resonance and Fabry-Pérot resonance, which is confirmed by the electric field distribution. Moreover, the effect of geometric parameters on absorption performance is analyzed. Finally, we discuss the influence of incident angle on the solar absorber. We believe this work could deepen the understanding of coupling resonance mode and guide the design of high-temperature solar absorbers.

1. Introduction

Energy is decisive in constraining global economic development in the coming decades [1]. Recent studies show that fossil energy, which can cause serious environmental problems, still accounts for more than 80% of global energy consumption. In contrast, as a promising renewable energy, solar energy has advantages in large storage capacity and wide distribution. Specifically, photothermal conversion is one of the most direct and effective ways to utilize solar energy. Concentrated photovoltaic systems use geometrical optical properties to converge low-density solar irradiation on a narrow photovoltaic cell, which effectively improves the conversion efficiency of the system [2–6]. However, the huge radiative heat flux will cause the system temperature to rise rapidly, which poses significant challenges for designing solar absorbers. Moreover, highly concentrated solar irradiation may damage the surface structure of the solar absorber [7,8]. Therefore, it is of great significance to investigate high-temperature resistant solar absorbers.

Metasurface, which exhibits exotic properties that are not found in nature, has numerous promising applications in imaging, sensing, and solar harvesting [9–23]. Particularly, solar absorbers based on metasurface have attracted significant attention because of their ability to absorb solar irradiation over a wide range of wavelengths. So far, numerous efforts have been devoted to the design of metasurface solar absorbers [24–44]. Charola et al. theoretically proposed and numerically analyzed a metasurface broadband absorber based on Au and Ti [45]. The results show that the absorber can achieve more than 95% broadband absorption between 550 and 651 THz. Heidari et al. designed a novel broadband, polarization-insensitive absorber [46]. An average absorption of more than 90% was achieved in the visible region. Azad et al. investigated a metasurface solar absorber consisting of eight pairs of gold nanoresonators [47]. Results show that the absorption was greater than 90% in the solar spectrum, and low emissivity was shown in the mid and far-infrared regions. Although all the above-proposed absorbers have good solar energy absorption performance, the research on high-temperature absorbers is highly desired and worth further exploration.

Here, the metasurface solar absorber is investigated, taking advantage of the high-temperature resistance characteristics of TiN and SiO_2. The absorber comprises a TiN substrate, SiO_2 layer, TiN layer, and TiN cylinder array. The total solar absorption (AM1.5 data) of the absorber is analyzed. The electric field distribution can reveal the high absorption performance of the metasurface absorber. Moreover, the geometric

* Corresponding author.
E-mail address: xiaohu.wu@iat.cn (X. Wu).

https://doi.org/10.1016/j.ijthermalsci.2023.108428
Received 4 February 2023; Received in revised form 18 April 2023; Accepted 15 May 2023
Available online 27 May 2023
1290-0729/

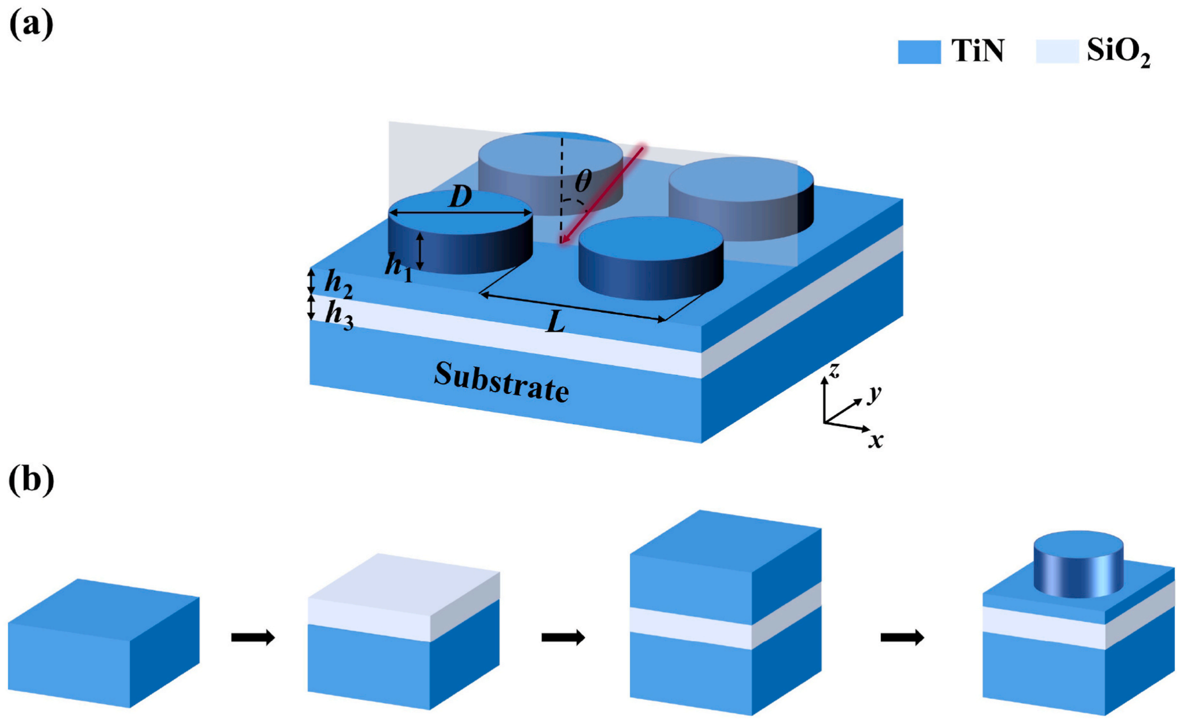

Fig. 1. (a) Schematic diagram of the proposed metasurface absorber. The period, diameter and height of the cylinder array structure are L, D, and h_1. The thicknesses of TiN and SiO_2 layer are h_2 and h_3. The light is incident obliquely from the air at angle of θ on the proposed metasurface absorber in the x-z plane. (b) Simple flowchart for the general fabrication procedure of the metasurface absorber.

parameters effect of the solar absorber on absorption performance is analyzed. Finally, we discuss the influence of incident angle on absorption performance for different polarizations.

2. Models and methods

Fig. 1(a) gives a schematic diagram of the proposed metasurface absorber based on the cylinder array. The high melting point materials TiN (2950 °C) and SiO_2 (1723 °C) are used. The absorber comprises a TiN substrate, SiO_2 layer, TiN layer and TiN cylinder arrays. Compared to absorbers formed by metallic nanoresonant cavities, TiN-based solar absorbers have greater thermal stability [48–50]. It can not only reduce the cost but also improve the high-temperature resistance of the absorber. The period is $L = 400$ nm. The diameter and height of the cylinder array are $D = 240$ nm, and $h_1 = 150$ nm. The thickness of the TiN layer and SiO_2 layer are $h_2 = 5$ nm and $h_3 = 170$ nm. The thickness of the TiN substrate is set as 500 nm to reduce the transmittance. The light is incident obliquely at angle of θ in the x-z plane for transverse magnetic (TM) or transverse electric (TE) polarization. Permittivities of TiN and SiO_2 can be found in Ref. [51]. The default conditions are the incidence angle $\theta = 0$ and TM polarization unless otherwise specified. Fig. 1(b) gives the general fabrication procedure of the metasurface absorber. First, the TiN substrate is deposited by magnetron sputtering. Followed by ultrasonic cleaning TiN substrate and using an ion beam sputter in the TiN substrate placed SiO_2 layer. Then, electron beam evaporation deposits a TiN layer on the SiO_2 layer. Finally, micro-cylinder arrays are fabricated on the TiN layer by UV lithography and reactive ion etching [52,53].

The spectral absorption performance is calculated by finite difference time domain method. In the simulation, the perfectly matched layer is used as boundary condition in the z-axis direction. For the case where the angle of incidence is 0, we use periodic boundary conditions in the x and y-axis directions. The Bloch boundary conditions are used when the light source is incident obliquely. Power monitors are arranged above the light source and below the absorber to detect reflections and transmissions. The operating environment of the absorber is air. The spectral absorption A_λ and average spectral absorption $A_{average}$ are expressed as:

$$A_\lambda = 1 - R_\lambda - T_\lambda \tag{1}$$

$$A_{average} = \frac{\int_{\lambda_1}^{\lambda_2} A_\lambda d\lambda}{\int_{\lambda_1}^{\lambda_2} d\lambda} \tag{2}$$

where R_λ and T_λ are spectral reflection and transmission; $\lambda_1 = 300$ nm and $\lambda_2 = 2500$ nm are the upper and lower limits of the operating wavelength of the metasurface absorber. Since the thickness of the TiN substrate is large enough, the transmission T_λ is almost 0. The total solar absorption α can be expressed as [54,55]:

$$\alpha = \frac{\int_{\lambda_1}^{\lambda_2} A_\lambda I_{AM1.5}(\lambda) d\lambda}{\int_{\lambda_1}^{\lambda_2} I_{AM1.5}(\lambda) d\lambda} \tag{3}$$

where $I_{AM1.5}(\lambda)$ is the spectral intensity of the solar irradiation (AM 1.5 data).

3. Results and discussions

To further highlight the advantages of the proposed metasurface absorber, we exhibit two structures: TiN layer/SiO_2 layer/TiN substrate (Case 1), TiN cylinder array/SiO_2 layer/TiN substrate (Case 2), as shown in Fig. 2(a). It can be seen that the TiN cylinder array (Case 1) and the TiN layer (Case 2) are not used in these two cases, compared to the provided absorber. Fig. 2(b) shows the spectral absorption of three cases at wavelength of 300–2500 nm. Case 1 has two absorption peaks at wavelengths of 390 nm and 920 nm, both with spectral absorptions above 0.99. These two absorption peaks are attributed to the intrinsic absorption of TiN (390 nm) and Fabry-Pérot resonance (920 nm). Notably, the structure has an absorption valley at wavelength of 600 nm with an absorption of only 0.43 due to the intrinsic loss of TiN. In Case 2,

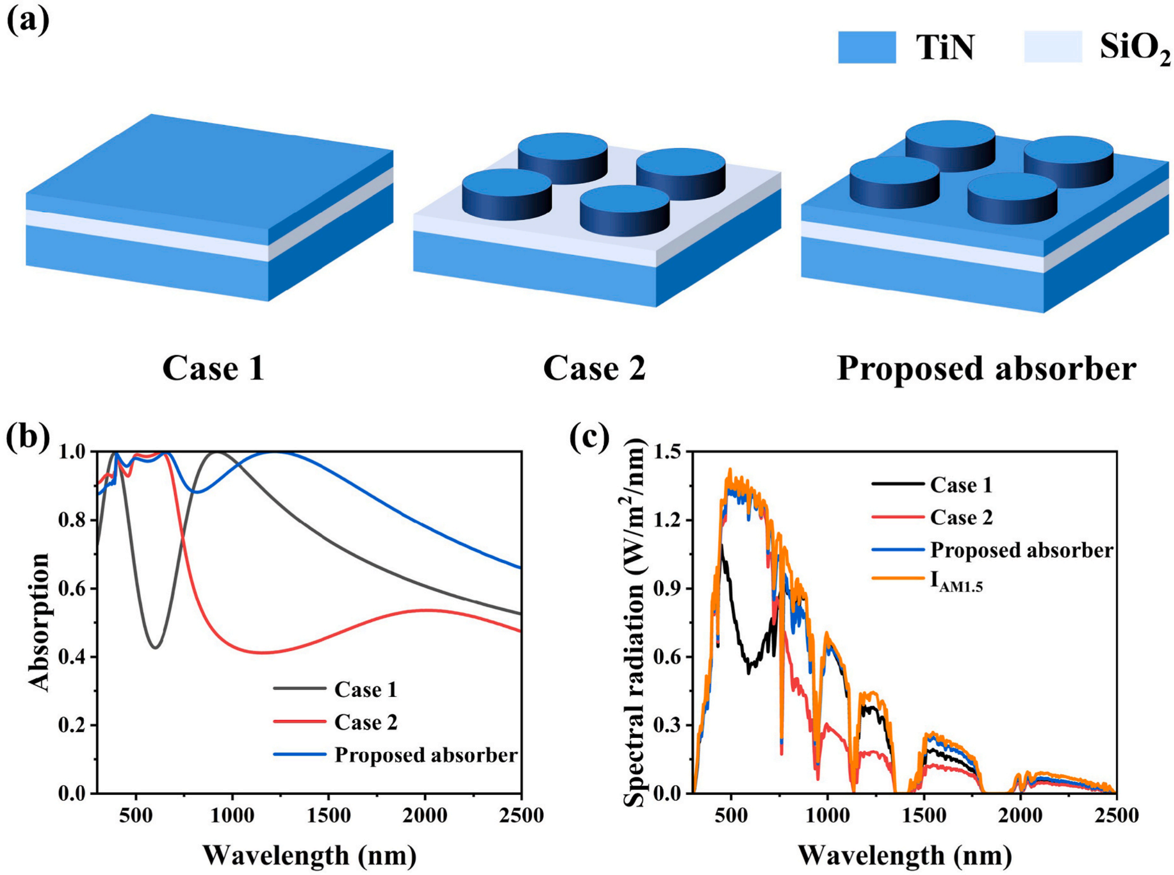

Fig. 2. (a) Comparison of three different structures of metasurface absorbers: TiN layer/SiO_2 layer/TiN substrate (Case 1), TiN cylinder array/SiO_2 layer/TiN substrate (Case 2), TiN cylinder array/TiN layer/SiO_2 layer/TiN substrate (Proposed absorber). (b) Spectral absorption and (c) spectral solar absorption (AM1.5 data) of three different structures at wavelength of 300–2500 nm.

the high absorption performance is mainly concentrated in the visible band, while the absorption in the near-infrared band is low. The proposed absorber fully uses the structural advantages of these two cases. Compared to Case 1, it effectively overcomes the absorption valley in the visible wavelength band. Compared to Case 2, it enhances the absorption in the near-infrared band. The average spectral absorption of the proposed metasurface absorber is 88.0%, which is 16.0% and 29.9% higher than the other two cases. Fig. 2(c) shows the spectral solar absorption of three cases at wavelength of 300–2500 nm. It can be seen that Case 1 has a large solar radiation loss in the visible band due to the existence of an absorption valley at the wavelength of 600 nm. In addition, for Case 2, the solar radiation in the near-infrared band is not well harvested. Combining the advantages of these two cases, the proposed absorber achieves up to 94.4% of total solar absorption, which is 20.3% and 21.5% higher than the other two cases.

To explain the potential mechanism of the high absorption performance of metasurface absorbers, we calculated the electric field distributions of different structures. Fig. 3(a) and Fig. 3(b) show electric field distributions of Case 1 at wavelengths of 600 nm, and 920 nm. Strong electric field region is concentrated in the air when the wavelength is 600 nm, which proves that the structure has a strong reflection. Therefore, there is an absorption valley at this wavelength caused by the inherent loss of TiN. When the wavelength is 920 nm, the strong electric field is located inside the absorber. The absorption peak can be attributed to the Fabry-Pérot resonance. The electric field in the air is close to 1, proving that the metasurface absorber at that wavelength almost completely absorbs the light. Fig. 3 (c) and 3(d) give electric field distributions of Case 2 at wavelengths of 600 nm, and 1160 nm. When the wavelength is 600 nm, a strong and symmetrical electric field is excited at the TiN/air interface above, indicating that the absorption peak can be explained as the combined effect of the intrinsic properties of TiN and surface plasmon resonance. When the wavelength is 1160 nm, the position of the strong electric field region decreases. Fig. 3(e) and (f) show electric field distributions of metasurface absorber at wavelengths of 600 nm, and 1220 nm. Note that the physical mechanism of the metasurface absorber at wavelength of 600 nm is similar to that in Fig. 3(c). When the wavelength is 1220 nm, the electric field is strongly excited at TiN/air interface as well as in the air. Due to the coupling effect of surface plasmon resonance and Fabry-Pérot resonance, the performance of absorber in the near-infrared region is significantly enhanced.

Moreover, the influence of geometric parameters on absorption performance is investigated. The effect of period L is shown in Fig. 4(a). As the increase of period, absorption in the visible region gradually increases, while absorption peak in the near-infrared region possesses blueshifts. It can be seen that the spectral absorption does not fluctuate greatly with the period. As shown in Fig. 4(b), the influence of the diameter of cylinder D presents an opposite phenomenon. The absorption performance in the visible region decreases, while the absorption peak in the near-infrared region possesses redshifts with increased diameter. The overall absorptive properties also changed little. Fig. 4(c) shows the influence of the height of cylinder h_1. The variation of the absorption curve is similar to the influence of diameter D. The influence of TiN layer thickness h_2 is shown in Fig. 4(d). When the TiN layer is not used, the absorption spectrum decreases obviously in the near-infrared region. The basic principles are discussed in detail in the previous section. When TiN layer thickness h_2 is not 0, the absorption bandwidth of the proposed metasurface absorber is weakened. One can see that the geometric parameters have little effect on the broadband absorption

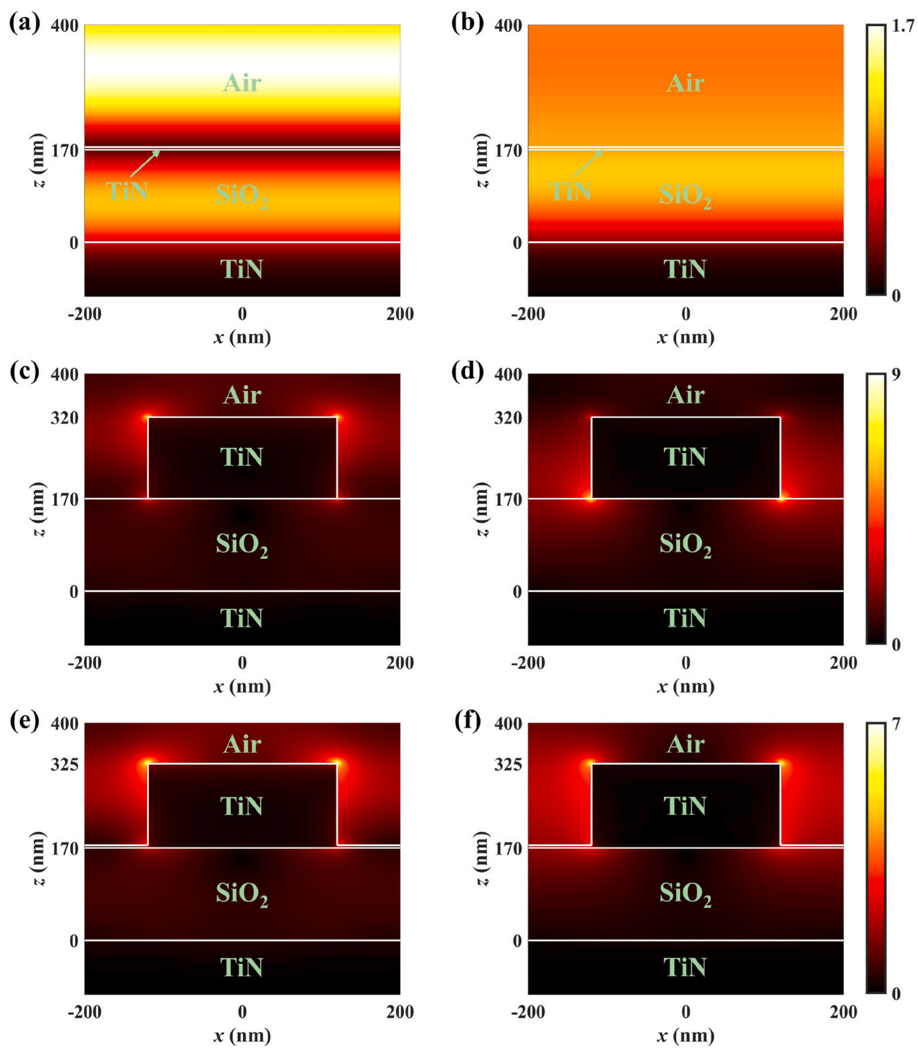

Fig. 3. Electric field distributions of Case 1 at wavelengths of (a) 600 nm, (b) 920 nm. Electric field distributions of Case 2 at wavelengths of (c) 600 nm, (d) 1160 nm. Electric field distributions of proposed metasurface absorber at wavelengths of (e) 600 nm, (f) 1220 nm.

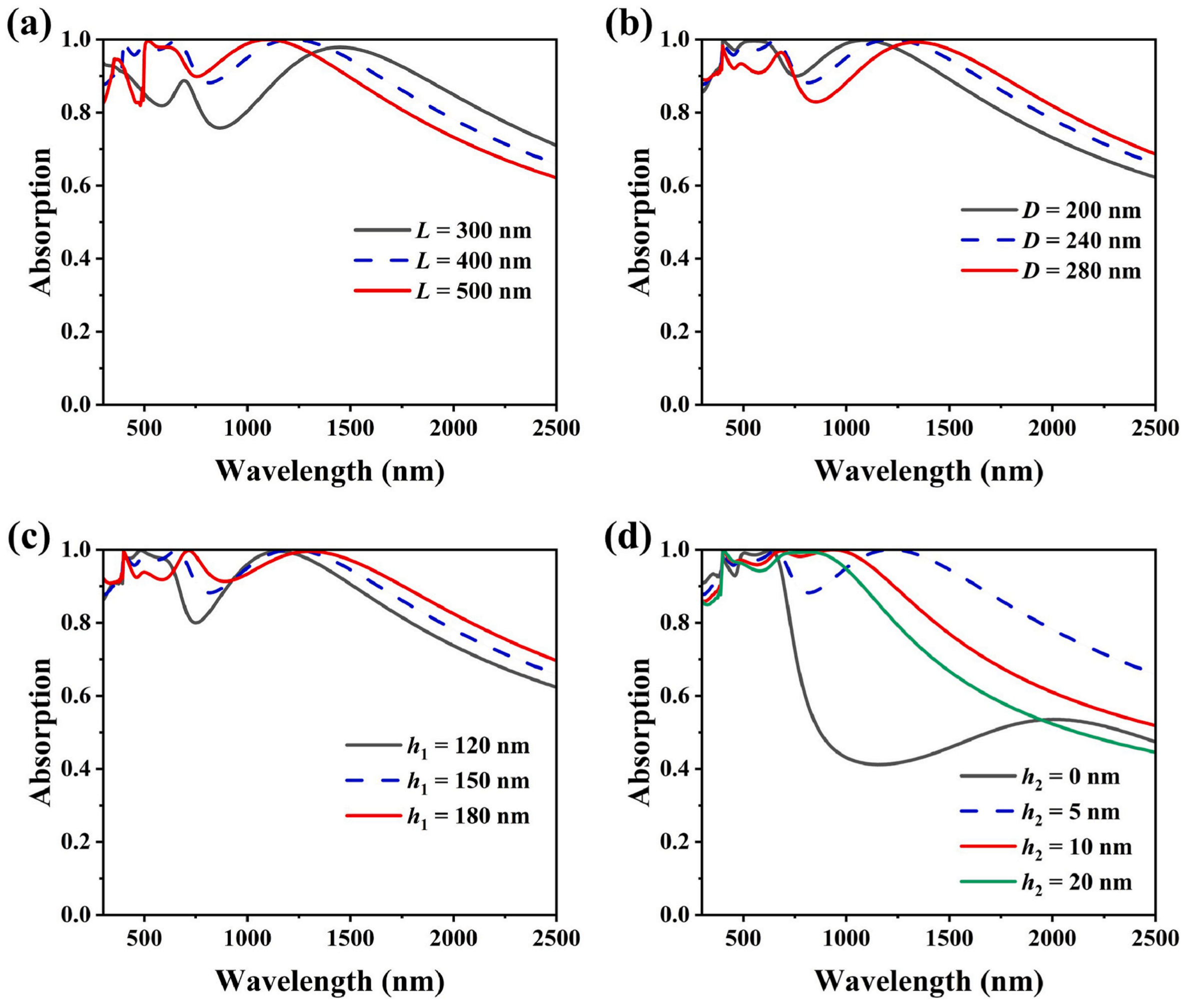

Fig. 4. Influence of geometric parameters on the spectral absorption of the proposed metasurface absorber: (a) period L, (b) diameter D of TiN cylinder, (c) height h_1 of TiN cylinder, and (d) thickness h_2 of TiN layer.

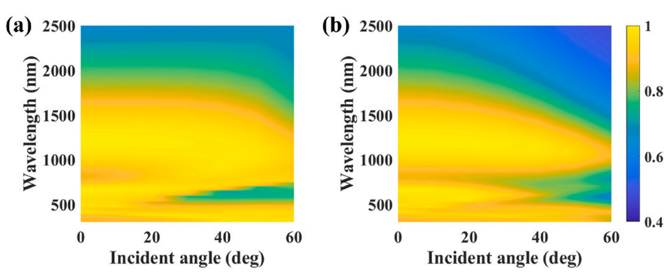

Fig. 5. Spectral absorption of proposed absorber versus incident angle for (a) TM, and (b) TE polarization.

performance of the proposed metasurface absorber. This indicates that the absorber has a large manufacturing tolerance, which is conducive to manufacturing the absorber in practical applications.

In practice, solar radiation is mainly divided into TM and TE polarization and the incident angle is uncertain. Therefore, it is essential to consider the effect of incident angle and polarization direction on the absorber performance. Fig. 5 (a) shows spectral absorption varies with the incident angle for TM polarization. It can be seen that the metasurface absorber is highly insensitive to the incident angle. When the incident angle is 60°, the average spectral absorption can achieve 0.81. Fig. 5 (b) shows the case for TE polarization. The average spectral absorption can be up to 0.68 when the incident angle is 60°. It can be seen that the overall absorption characteristics of the absorber exhibit a greater angular insensitivity to TM-polarized light than TE-polarized light in the solar irradiation bands. Moreover, we considered the effect of the polarization angle as shown in Fig. 6. The results show that the proposed metasurface absorber is polarization-independent, which can be explained by the isotropy of the material and the symmetry of the structure.

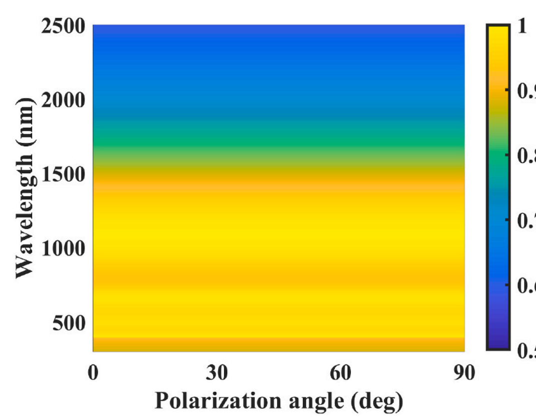

Fig. 6. Spectral absorption of proposed absorber versus polarization angle for normal incidence.

4. Conclusions

We propose a high-temperature resistant metasurface solar absorber based on TiN cylinder arrays. The average spectral absorption is 0.88, and the total solar absorption is 0.94 at 300–2500 nm. The high absorption performance of the metasurface absorber can be explained as the coupling effect of surface plasmon resonance and Fabry-Pérot resonance, which is determined by analyzing the electric field distribution. The discussion in geometric parameters effect indicates that the absorber has a large manufacturing tolerance, which is conducive to manufacturing the absorber in practical applications. In addition, we find that the proposed absorber still has superior performance (0.81 for TM polarization, 0.68 for TE polarization) at a large incident angle of 60°. We believe this work will guide us in the design of high-temperature solar absorbers.

Declaration of competing interest

The authors declare that they have no known competing financial interests or personal relationships that could have appeared to influence the work reported in this paper.

Data availability

Data will be made available on request.

Acknowledgment

This work is supported by the National Natural Science Foundation of China (52106099), the Natural Science Foundation of Shandong Province (ZR2022QE045, ZR2022YQ57), and the Taishan Scholars Program.

References

[1] M. Ball, M. Wietschel, The future of hydrogen–opportunities and challenges, Int. J. Hydrogen Energy 34 (2009) 615–627.
[2] F. Rubino, P. Poza, G. Pasquino, P. Carlone, Thermal surface plasmon resonanceay processes in concentrating solar power technology, Metals 11 (2021) 1377.
[3] Y. He, Y. Qiu, K. Wang, F. Yuan, W. Wang, M.J. Li, J.Q. Guo, Perspective of concentrating solar power, Energy 198 (2020), 117373.
[4] G. Li, Q. Xuan, G. Pei, Y. Su, J. Ji, Effect of non-uniform illumination and temperature distribution on concentrating solar cell - a review, Energy 144 (2018) 1119–1136.
[5] R. Poeira, A. Perez-Rodriguez, A. Prot, M. Alves, P. Dale, S. Sadewasser, Direct fabrication of arrays of Cu (In,Ga)Se_2 micro solar cells by sputtering for micro-concentrator photovoltaics, Mater. Des. 225 (2023), 111597.
[6] M. Wiesenfarth, M. Steiner, H. Helmers, A.W. Bett, Voltage losses due to the perimeter and dark area in micro-concentrator solar cells, Sol. Energy Mater. Sol. Cell. 219 (2021), 110791.
[7] C. Sun, Y. Zou, C. Qin, B. Zhang, X. Wu, Temperature effect of photovoltaic cells: a review, Adv. Compos. Hybrid Mater. 5 (2022) 2675–2699.
[8] X. Lu, Y. Zhao, Z. Wang, J. Zhang, Y. Song, Influence of environmental temperature and device temperature difference on output parameters of c-Si solar cells, Sol. Energy 136 (2016) 333–341.
[9] P. Agarwal, K. Kishor, R.K. Sinha, Ultrasensitive dual-band terahertz metasurface sensor based on all InSb resonator, Opt Commun. 522 (2022), 128667.
[10] R. Bilal, M. Baqir, P. Choudhury, M. Naveed, M. Ali, A. Rahim, Ultrathin broadband metasurface-based absorber comprised of tungsten nanowires, Results Phys. 19 (2020), 103471.
[11] R. Kumar, B. Singh, P. Pandey, Broadband metamaterial absorber in the visible region using a petal-shaped resonator for solar cell applications, Phys. E Low-dimens. Syst. Nanostruct. 142 (2022), 115327.
[12] H. Liu, Q. Ai, M. Ma, Z. Wang, M. Xie, Prediction of spectral absorption of anisotropic α-MoO_3 nanostructure using deep neural networks, Int. J. Therm. Sci. 177 (2022), 107587.
[13] F. Zhao, J. Lin, Z. Lei, Z. Yi, F. Qin, J. Zhang, L. Liu, W. Yang, P. Wu, Realization of 18.97% theoretical efficiency of 0.9 μm thick c-Si/ZnO heterojunction ultrathin-film solar cells via surface plasmon resonance enhancement, Phys. Chem. Chem. Phys. 24 (2022) 4871–4880.
[14] Z. Zheng, Y. Luo, H. Yang, Z. Yi, J. Zhang, Q. Song, W. Yang, C. Liu, X. Wu, P. Wu, Thermal tuning of terahertz metamaterial absorber properties based on VO 2, Phys. Chem. Chem. Phys. 24 (2022) 8846–8853.
[15] S. Xiao, T. Wang, T. Liu, X. Yan, Z. Li, C. Xu, Active modulation of electromagnetically induced transparency analogue in terahertz hybrid metal-graphene metamaterials, Carbon 126 (2018) 271–278.
[16] S. Xiao, T. Wang, T. Liu, C. Zhou, X. Jiang, J. Zhang, Active metamaterials and metadevices: a review, J. Phys. Appl. Phys. 53 (2020), 503002.
[17] J. Wu, Y. Sun, B. Wu, C. Sun, X. Wu, Perfect metamaterial absorber for solar energy utilization, Int. J. Therm. Sci. 179 (2022), 107638.
[18] H. Liu, M. Xie, Q. Ai, Z. Yu, Ultra-broadband selective absorber for near-perfect harvesting of solar energy, J. Quant. Spectrosc. Radiat. Transf. 266 (2021), 107575.
[19] S. Sun, D. Zhang, B. Wu, H. Liu, B. Yang, X. Wu, Metasurfaces assisted twisted α-MoO_3 for spinning thermal radiation, Micromachines 13 (2022) 1757.
[20] S. Liang, F. Xu, H. Yang, S. Cheng, W. Yang, Z. Yi, Q. Song, P. Wu, J. Chen, C. Tang, Ultra long infrared metamaterial absorber with high absorption and broad band based on nano cross surrounding, Opt Laser. Technol. 158 (2023), 108789.
[21] Q. Shangguan, Y. Zhao, Z. Song, J. Wang, H. Yang, J. Chen, C. Liu, S. Cheng, W. Yang, Z. Yi, High sensitivity active adjustable graphene absorber for refractive index sensing applications, Diam. Relat. Mater. 128 (2022), 109273.
[22] F. Zhou, F. Qin, Z. Yi, W. Yao, Z. Liu, X. Wu, P. Wu, Ultra-wideband and wide-angle perfect solar energy absorber based on Ti nanorings surface plasmon resonance, Phys. Chem. Chem. Phys. 23 (2021) 17041–17048.
[23] H. Chen, Z. Chen, H. Yang, L. Wen, Z. Yi, Z. Zhou, B. Dai, J. Zhang, X. Wu, P. Wu, Multi-mode surface plasmon resonance absorber based on dart-type single-layer graphene, RSC Adv. 12 (2022) 7821–7829.
[24] L. Long, Y. Yang, L. Wang, Simultaneously enhanced solar absorption and radiative cooling with thin silica micro-grating coatings for silicon solar cells, Sol. Energy Mater. Sol. Cell. 197 (2019) 19–24.
[25] H. Liu, B. Wu, B. Yang, Q. Ai, M. Xie, X. Wu, Gradient index effect assisted anisotropic broadband absorption in α-MoO_3 metamaterial, Appl. Opt. 11 (2023) 2711–2719.
[26] J. Wu, Y. Sun, B. Wu, C. Sun, X. Wu, Broadband and wide-angle solar absorber for the visible and near-infrared frequencies, Sol. Energy 238 (2022) 78–83.
[27] Q. Shangguan, Z.H. Chen, H. Yang, S.B. Cheng, W.X. Yang, Z. Yi, X.W. Wu, S. F. Wang, Y.G. Yi, P.H. Wu, Design of ultra-narrow band graphene refractive index sensor, Sensors 22 (2022) 6483.
[28] Z. Zheng, Y. Zheng, Y. Luo, Z. Yi, J. Zhang, Z. Liu, W. Yang, Y. Yu, X. Wu, P. Wu, Switchable terahertz device combining ultra-wideband absorption and ultra-wideband complete reflection, Phys. Chem. Chem. Phys. 24 (2022) 2527–2533.
[29] J. Hao, L. Zhou, M. Qiu, Nearly total absorption of light and heat generation by plasmonic metasurface, Phys. Rev. B 83 (2011), 165107.
[30] M. Xu, L. Guo, P. Zhang, Y. Qiu, Q. Li, J. Wang, Near-perfect spectrally-selective metasurface solar absorber based on tungsten octagonal prism array, RSC Adv. 12 (2022), 16823.
[31] C. Sun, H. Liu, B. Yang, K. Zhang, B. Zhang, X. Wu, Ultra-broadband and wide-angle absorber based on TiN metamaterial for solar harvesting, Phys. Chem. Chem. Phys. 25 (2023) 806–812.
[32] H. Li, H. Zhou, G. Wei, H. Xu, M. Qin, J. Liu, F. Wu, Photonic spin-selective perfect absorptance on planar metasurfaces driven by chiral quasi-bound states in the continuum, Nanoscale 15 (2023) 6636–6644.
[33] Q. Liang, H. Duan, X. Zhu, X. Chen, X. Xia, Solar thermal absorber based on dielectric filled two-dimensional nickel grating, Opt. Mater. Express 9 (2019) 3193–3203.
[34] S. Patel, S. Charola, J. Parmar, M. Ladumor, Broadband metasurface solar absorber in the visible and nearinfrared region, Mater. Res. Express 6 (2019), 086213.
[35] J. Wu, D. Huang, B. Wu, X. Wu, Extremely broadband light absorption by bismuth-based Metasurface involving hybrid resonances, Phys. Chem. Chem. Phys. 24 (2022) 21612–21616.
[36] R. Jadeja, S. Charola, S.K. Patel, J. Parmar, Numerical investigation of graphene-based efficient and broadband metasurface for terahertz solar absorber, J. Mater. Sci. 55 (2020) 3462–3469.
[37] P. Wu, S. Dai, X. Zeng, N. Su, L. Cui, H. Yang, Design of ultra-high absorptivity solar absorber based on Ti and TiN multilayer ring structure, Int. J. Therm. Sci. 183 (2023), 107890.
[38] M. Alsharari, B. Han, S. Patel, J. Surve, K. Aliqab, A. Armghan, A highly efficient infinity-shaped large angular-and polarization-independent metamaterial absorber, Symmetry 15 (2023) 352.
[39] S. Patel, J. Surve, J. Parmar, V. Katkar, R. Jadeja, S. Taya, K. Ahmed, Graphene-based metasurface solar absorber design for the visible and near-infrared region with behavior prediction using polynomial regression, Optik 262 (2022), 169298.
[40] S. Patel, J. Surve, P. Prajapati, S. Taya, Design of an ultra-wideband solar energy absorber with wide-angle and polarization independent characteristics, Opt. Mater. 131 (2022), 112683.
[41] S. Patel, A. Udayakumar, G. Mahendran, B. Vasudevan, J. Surve, J. Parmar, Highly efficient, perfect, large angular and ultrawideband solar energy absorber for UV to MIR range, Sci. Rep. 12 (2022), 18044.
[42] Y. Zheng, P. Wu, H. Yang, Z. Yi, Y. Luo, L. Liu, Q. Song, M. Pan, J. Zhang, P. Cai, High efficiency Titanium oxides and nitrides ultra-broadband solar energy absorber and thermal emitter from 200 nm to 2600 nm, Opt Laser. Technol. 150 (2022), 108002.
[43] S. Patel, J. Surve, V. Katkar, J. Parmar, Optimization of metamaterial-based solar energy absorber for enhancing solar thermal energy conversion using artificial intelligence, Adv. Theor. Simulat. 5 (2022), 2200139.
[44] F. Qin, F. Xu, J. Liu, P. Hu, Z. Yi, L. Liu, H. Yang, J. Zhang, M. Pan, P. Wu, Broadband solar absorbers with excellent thermal radiation efficiency based on W-Al_2O_3 stack of cubes, Int. J. Therm. Sci. 179 (2022), 107683.

[45] S. Charola, S. Patel, J. Parmar, R. Jadeja, Broadband and angle-insensitive metasurface solar absorber, Opt. Quant. Electron. 54 (2022) 348.
[46] M. Heidari, S. Sedighy, Broadband wide-angle polarization-insensitive metasurface solar absorber, J. Opt. Soc. Am. A 35 (2018), 314236.
[47] A. Azad, W. Kort-Kamp, M. Sykora, N. Weisse-Bernstein, T. Luk, A. Taylor, D. Dalvit, H. Chen, Metasurface broadband solar absorber, Sci. Rep. 6 (2015), 20347.
[48] H. Zhong, Z. Liu, P. Tang, X. Liu, X. Zhan, P. Pan, C. Tang, Thermal-stability resonators for visible light full-spectrum perfect absorbers, Sol. Energy 208 (2020) 445–450.
[49] S. Ishii, R. Kamakura, H. Sakamoto, T. Dao, S. Shinde, T. Nagao, K. Fujita, K. Namura, M. Suzuki, S. Murai, K. Tanaka, Demonstration of temperature-plateau superheated liquid by photothermal conversion of plasmonic titanium nitride nanostructures, Nanoscale 10 (2018), 18451.
[50] Z. Yang, S. Ishii, A. Doan, S. Shinde, T. Dao, Y. Lo, K. Chen, T. Nagao, Narrow-Band thermal emitter with titanium nitride thin film demonstrating high temperature stability, Adv. Opt. Mater. 8 (2020), 1900982.
[51] E. Palik, Handbook of Optical Constants of Solids, Academic Press, Cambridge, MA, USA, 1998.
[52] E. Akerboom, T. Veeken, C. Hecker, J. van de Groep, A. Polman, Passive radiative cooling of silicon solar modules with photonic silica microcylinders, ACS Photonics 9 (2022) 3831–3840.
[53] R. Fang, Z. Yu, Y. Lin, Lithography-free fabrication and optical characterizations of nanotextured nickel dewetting thin film for broadband absorbers, Nano Futures 6 (2022), 035003.
[54] Air Mass 1.5 Spectra, American society for testing and materials (ASTM), Available from: http://rredc.nrel.gov/solar/spectra/am1.5/.
[55] P. Yu, H. Yang, X. Chen, Z. Yi, W. Yao, J. Chen, Y. Yi, P. Wu, Ultra-wideband solar absorber based on refractory titanium metal, Renew. Energy 158 (2020) 227–235.